AIAA JOURNAL
Vol. 30, No. 11, November 1992

Hybrid Grid Approach to Study Dynamic Stall

Taekyu Reu* and Susan X. Ying†
Florida State University, Tallahassee, Florida 32306

A hybrid structured and unstructured grid scheme is developed to study dynamic stall over an airfoil in a wind tunnel. The unsteady Navier-Stokes equations are solved implicitly using this hybrid grid scheme. Results are compared with experimental data. Additionally, they reveal informative details of the flowfield physics associated with dynamic stall.

Introduction

THE objective of this work is to develop an efficient hybrid grid algorithm to study the dynamic stall over a pitching airfoil. In particular, this numerical simulation will be used to predict the physics including wind-tunnel wall interference.

The dynamic stall over a pitching airfoil is characterized by unsteady flow separation and the formation of a leading-edge vortex. Development of these unsteady phenomena produces significant differences in the aerodynamic performances compared to steady flows. Understanding dynamic stall is important for designing aircraft, rotor blades, and wind turbines. The control and utilization of the aerodynamic loads introduced by these physical phenomena requires insight into the unsteady flowfield.

At the Florida State University, the particle image displacement velocimetry (PIDV) technique[1] has been developed to measure the unsteady flowfield velocity vectors. The complexity and rapidity of the flow development makes this experiment very challenging and difficult. Furthermore, the experimental study of dynamic stall over an airfoil is complicated by the wind-tunnel wall interference. The measurements must be corrected on the basis of steady calibrations. Although the PIDV data is not yet available, our numerical solutions will be used to predict the wall interference and compared to the PIDV measurements. Numerical flow visualization will also be used to study flowfield details of dynamic stall. The AGARD data,[2] already corrected by calibrations, is used to verify the computed results in this work.

Numerical simulation of a pitching airfoil in a wind tunnel presents several challenges. The first and the most important one is to capture the unsteady flow separation phenomenon. This requires accurately resolving the unsteady boundary-layer development around the airfoil. The second challenge is simulating the formation and evolution of the vortical structures on the leeward side of the airfoil. The third challenge, also identified by a number of researchers,[3-5] is the effect of compressibility in dynamic stall; in particular, the effects of the shock wave formation on the leading-edge vortex. This issue will not be addressed in this work, rather a Mach 0.3 flow is investigated. Last, moving and confining the airfoil between the wind-tunnel walls requires a delicate numerical approach. That is, one needs to regrid or interpolate at each time step. Consequently, in addition to solving the unsteady flow equations, a considerable amount of CPU time will be used for interpolation or to compute the transient grids. These physical and numerical challenges necessitate formulation of an efficient Navier-Stokes algorithm that integrates the unsteady grid strategies to the flow solution procedure.

In this research, the approach is to couple structured grids and unstructured grids. The motivation in this hybrid grid scheme is to explore ways that can efficiently and accurately simulate the complex physical phenomena due to dynamic stall. However, this method is not limited to simulating dynamic stall. This hybrid grid scheme can be applied to many internal unsteady flow problems, such as the flow around compressor or turbine blades in jet engines. The grid topology for simulating a pitching airfoil in a wind tunnel is not such a complex one. Yet comparing to a general single-grid approach, such as an adaptive remeshing finite element method,[6] this hybrid grid approach will be still less expensive for resolving the unsteady boundary layers. That is, by utilizing a structured, highly stretched, body-conforming grid around the airfoil, the gradients in the wall region can be very efficiently resolved. This is critical in simulating the physics of unsteady viscous flows.

In contrast to the single adaptive unstructured grid approach, there are also multizone patched grid methods and overset grid methods. These methods employ multiple structured grids for unsteady Navier-Stokes simulations. It has been demonstrated[7,8] that these methods can simulate the unsteady motion where one component moves with respect to the others. Nevertheless, the interpolation procedure for these methods is not vectorizable. Consequently, the computation time required for interpolation can be comparable to that of the flow solver at each time step, especially for the overset grid case. The approach for this work is similar to the multizone patched grid method. The major difference is in the application of unstructured grids. At each time step, an unstructured grid is used to patch the structured grids, thereby avoiding the excessive time necessary for interpolation. This approach will be referred to as the dynamic structured and unstructured grid (DSUG) method. The tradeoff here is in the grid generation at each time step. Again, it should be noted that, even though for this particular problem the geometries do not necessitate the use of an unstructured grid, the DSUG method can be readily generalized for more complex unsteady problems, and this work is only a start.

Although the DSUG approach can be very general and robust for modeling the flow over a pitching airfoil in wind tunnel, one can employ a simpler but less general method. This method uses rigid patched grids, allowing the inner grid to rotate while the outer grid stays fixed. As a result, there is a circular slip boundary in the domain and flow variables are interpolated across this boundary. This approach has been investigated by Rai,[9] and the DSUG approach will be compared to it. However, in this work, the slip boundary is embedded in the unstructured grid domain, different from that of Ref. 9. This procedure will be referred to as the patched

Presented as Paper 91-0599 at the AIAA 28th Aerospace Sciences Meeting, Reno, NV, Jan. 7-10, 1991; received June 28, 1991; revision received March 30, 1992; accepted for publication April 10, 1992.

*Supercomputer Computations Research Institute; currently Research Scientist, BAe, North Humberside, UK. Member AIAA.

†Assistant Professor, Supercomputer Computations Research Institute, Mechanical Engineering Department FAMU/FSU. Member AIAA.

structured and unstructured grid (PSUG) approach. Figures 1a and 1b show a comparison of photographs (at $\alpha = 3.82$ deg) of grids around the airfoil for these two approaches. In the next section, the numerical method will be described. Then the DSUG and PSUG approaches will be compared in terms of coding complexity and computational effort for an inviscid simulation. Finally, the results of dynamic stall at a reduced frequency of 0.02546, flow Mach number 0.3, and Reynolds number 2.7×10^6 are presented.

Numerical Method

The two-dimensional Navier-Stokes equations in nondimensionalized integral form are solved. These equations in Cartesian coordinates are given by

$$\frac{\partial}{\partial t}\iint_{\Omega} Q\,dA + \oint_{\partial\Omega} (F\,dy - G\,dx) = 0 \tag{1}$$

where Q is the conservative variables vector consisting of density, x and y momentums, and total energy per unit mass. The flux vectors F and G include both inviscid and viscous terms.

Spatial Discretization

An upwind cell-centered finite volume method is used to evaluate the flux integral in Eq. (1). For an arbitrary kth cell with edges e_j, Eq. (1) can be written in a semidiscretized form as

$$\left(\frac{\partial \hat{Q}V}{\partial t}\right)_k + \sum_{j=1}^{n} (F\Delta y - G\Delta x)_{e_j} = 0 \tag{2}$$

where $\hat{Q}$ is the cell averaged value of the conservative variables vector, and V is the area of the kth cell such that $\hat{Q}V = \int_V Q\,dV$. The summation of the fluxes in Eq. (2) is over

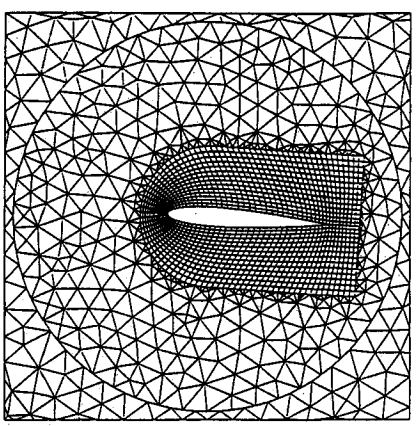

a) Details of an inviscid grid around the airfoil for the PSUG approach

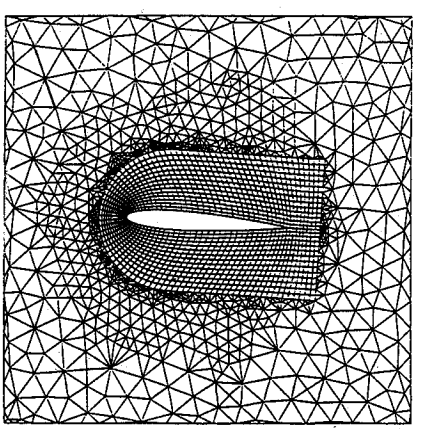

b) Details of an inviscid grid around the airfoil for the DSUG approach

Fig. 1 Comparison of the hybrid grid approaches at $\alpha = 3.82$ deg.

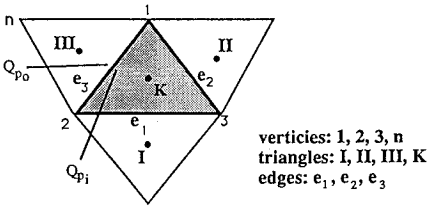

Fig. 2 Variables definition on the unstructured grid.

the cell faces (or edges), where n is 3 for a triangular cell and 4 for a rectangular cell.

For computing the inviscid flux terms on the structured grid, primitive cell-center variables $\hat{Q}_p$ (includes density, x and y components of velocity and pressure) are extrapolated to the cell interface (edge) by using an upwind-biased interpolation.[10] Roe's flux-difference scheme[11] is used for flux formulation. A similar approach is applied to compute the flux terms on the unstructured grid. As illustrated in Fig. 2, variables at the edge e_3 inside the kth triangle $\hat{Q}_{pi}$ are obtained using $\hat{Q}_K$, $\hat{Q}_{III}$, and $\hat{Q}_3$. Similarly, variables at the edge e_3 just outside the kth triangle $\hat{Q}_{po}$ are obtained using $\hat{Q}_K$, $\hat{Q}_{III}$, and $\hat{Q}_n$. The vertex variables such as $\hat{Q}_1$ and $\hat{Q}_n$ are obtained by averaging cell values around vertices. Since the viscous phenomenon in dynamic stall originates from the airfoil surface, and it is most dominant near the airfoil, viscous terms are evaluated only in the C grid around the airfoil. This inviscid/viscous approach can be found in Ref. 12 for steady-state cases. Second-order central differencing is used for all viscous terms, and the Baldwin-Lomax eddy-viscosity model[13] is employed for turbulent flow simulations.

Temporal Discretization

The semidiscrete governing equation (2) can be written in an operator form as

$$L(\hat{Q}) = \frac{\partial(\hat{Q}V)}{\partial t} + R(\hat{Q}) = 0 \tag{3}$$

Applying the Euler implicit method to this equation yields

$$L(\hat{Q}^{n+1}) = R(\hat{Q}^{n+1}) + (I/\Delta t)\{[1 + (\phi/2)](\hat{Q}V)^{n+1} - (1 + \phi)(\hat{Q}V)^n + (\phi/2)(\hat{Q}V)^{n-1}\} \tag{4}$$

This equation is first-order time accurate when $\phi = 0$ and second-order time accurate when $\phi = 1$. It can be solved iteratively by using the Newton's method. Rearranged in Delta form, Eq. (4) becomes

$$\left[\left(1 + \frac{\phi}{2}\right)\frac{V^{n+1}}{\Delta t} - \frac{\partial R(\hat{Q}^l)}{\partial \hat{Q}}\right]\Delta\hat{Q}^l = -R(\hat{Q}) - \frac{I}{\Delta t}\left[\left(1 + \frac{\phi}{2}\right)\hat{Q}^l V^{n+1} - (1 + \phi)(\hat{Q}V)^n + \frac{\phi}{2}(\hat{Q}V)^{n-1}\right] \tag{5}$$

where l is the subiteration index in each time step. The unknown vector $\Delta\hat{Q}^l$ is defined as $\Delta\hat{Q}^l = \hat{Q}^{l+1} - \hat{Q}^l$. At convergence of each time step, $\Delta\hat{Q}^l = 0$ and $\hat{Q}^l = \hat{Q}^{n+1}$. Local time steps are used to accelerate the convergence rate for the subiterations.

To further accelerate the solution procedure, the left-hand side of Eq. (5) is factored using the approximate factorization method[14] for the structured grid. For the unstructured grid, vectorization is achieved by utilizing a multicoloring method.[15]

Domain Decomposition

The physical space is split into several subdomains, each having a simple grid topology (see Fig. 3). Body-conforming structured grids are generated to enclose the wall regions in-

cluding the airfoil surface (subdomains II, III, and VI in Fig. 3). Each of these grids is generated independently and a gap is left between subdomain boundaries. An elliptic grid generator[16] was used for the C grid surrounding the airfoil. Subdomains I and VII are filled by simple Cartesian grids. It is trivial to generate these Cartesian grids, and they do not require metrics computation in solving the conservation laws. The gap between the body-conforming grid and the Cartesian grids is filled with an unstructured grid. The unstructured grid is generated using the Delaunay triangulation.[17] This grid is initially generated from boundary node points, and new node points are added at the center of the triangles that have larger cell area than the expected value. This is repeated until an acceptable unstructured grid is obtained and Laplacian smoothing[18] is used at each iteration.

Since the C grid and the inner unstructured grid rotate as a rigid body in the PSUG approach, remeshing is not required at each time step. However, in the DSUG case, the unstructured grid must be generated at each time step as the airfoil and the C grid rotate. To compute the grid at each time step, locations of new node points are obtained by modeling cell edges as springs with the spring stiffness inversely proportional to the edge length.[19]

Boundary Conditions

Characteristic boundary conditions based on Riemann invariants are used for inflow and outflow boundaries. Tangential boundary conditions are applied for the wind-tunnel walls. On the airfoil surface, no-slip boundary conditions are applied. At the subdomain interfaces for the DSUG approach, no interpolation is required. At the slip boundary between the moving grid and stationary grid for the PSUG approach, conservative variables are interpolated based on arc length, as in Ref. 9.

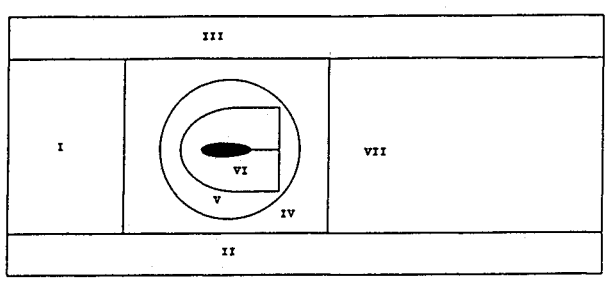

a) PSUG topology

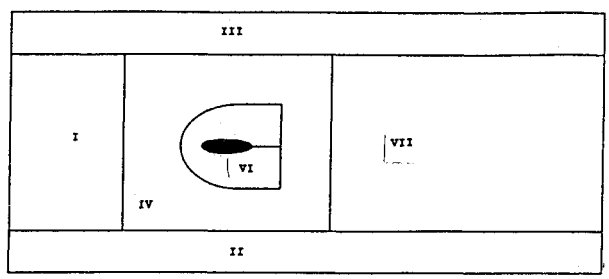

b) DSUG topology

Fig. 3 Subdomains of grid topology.

Results and Discussions

Two cases of flow simulation are presented here. The first simulation assumes inviscid flow, and the calculations are carried out using both DSUG and PSUG approaches. For viscous computation, however, there will be large grid discontinuity across the slip boundary in the PSUG approach. Although the interpolation procedure across this boundary is conservative, the PSUG approach will not be adequate for the prediction of the unsteady wake flow. Hence, only the DSUG approach is employed for simulating the physics of dynamic stall. The results for each case are obtained by starting from a converged steady solution at zero angle of attack. The airfoil is pitched up about its quarter-chord point. The pitching rate is prescribed in terms of reduced frequency, κ, defined as

$$\kappa = \dot{\alpha} c / V_\infty$$

where $\dot{\alpha}$ is the angular velocity, c the airfoil chord length, and V_∞ the freestream velocity.

Case 1: $M_\infty = 0.611$, $\kappa = 0.01492$

The airfoil is pitched up from 0 to 15 deg. Table 1 shows a summary of the number of grid points (or cells) for each domain corresponding to the DSUG and PSUG approaches shown in Fig. 3. It should be noted that the number of cells and node points for the unstructured grid region are not the same for the two approaches. This is because there is a circular slip boundary in the PSUG approach but not in the DSUG approach.

Identical solutions are obtained using PSUG and DSUG approaches. Figure 4 shows the normal force coefficient vs angle of attack for both numerical results and experimental data. Numerical results include both simulations with wind-tunnel wall and without wall assumption. Experimental data include the dynamic pitch-up as well as quasistatic measurements. These data indicate a quasistatic stall angle of attack (α_{qs}) at 2 deg earlier than the dynamic stall angle of attack ($\alpha_d = 10.4$ deg). It can be seen that before the dynamic stall ($\alpha < \alpha_d$) solutions without wall effect show very good agreement with the experimental data, whereas those with wall effect differ from the experimental data up to 15% (maximum at $\alpha = \alpha_d$). The good agreement is expected, since before the flow separates from the leading edge it is essentially inviscid.

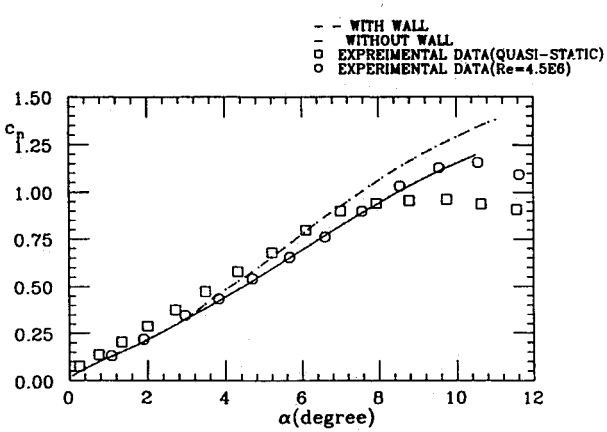

Fig. 4 Normal force coefficient hysteresis vs angle of attack for inviscid flow simulation at $M_\infty = 0.611$ and $\kappa = 0.01492$.

Table 1 Number of grid points and cells in each subdomain

	I	II	III	IV	V	VI	VII
PSUG[a]	24 × 19	101 × 7	101 × 7	398 cells, 262 nodes	694 cells, 433 nodes	95 × 15	58 × 19
DSUG[b]	24 × 19	101 × 7	101 × 7	1838 cells, 1018 nodes	0	95 × 15	58 × 19

[a]PSUG = patch structured and unstructured grid.
[b]DSUG = dynamic structured and unstructured grid.

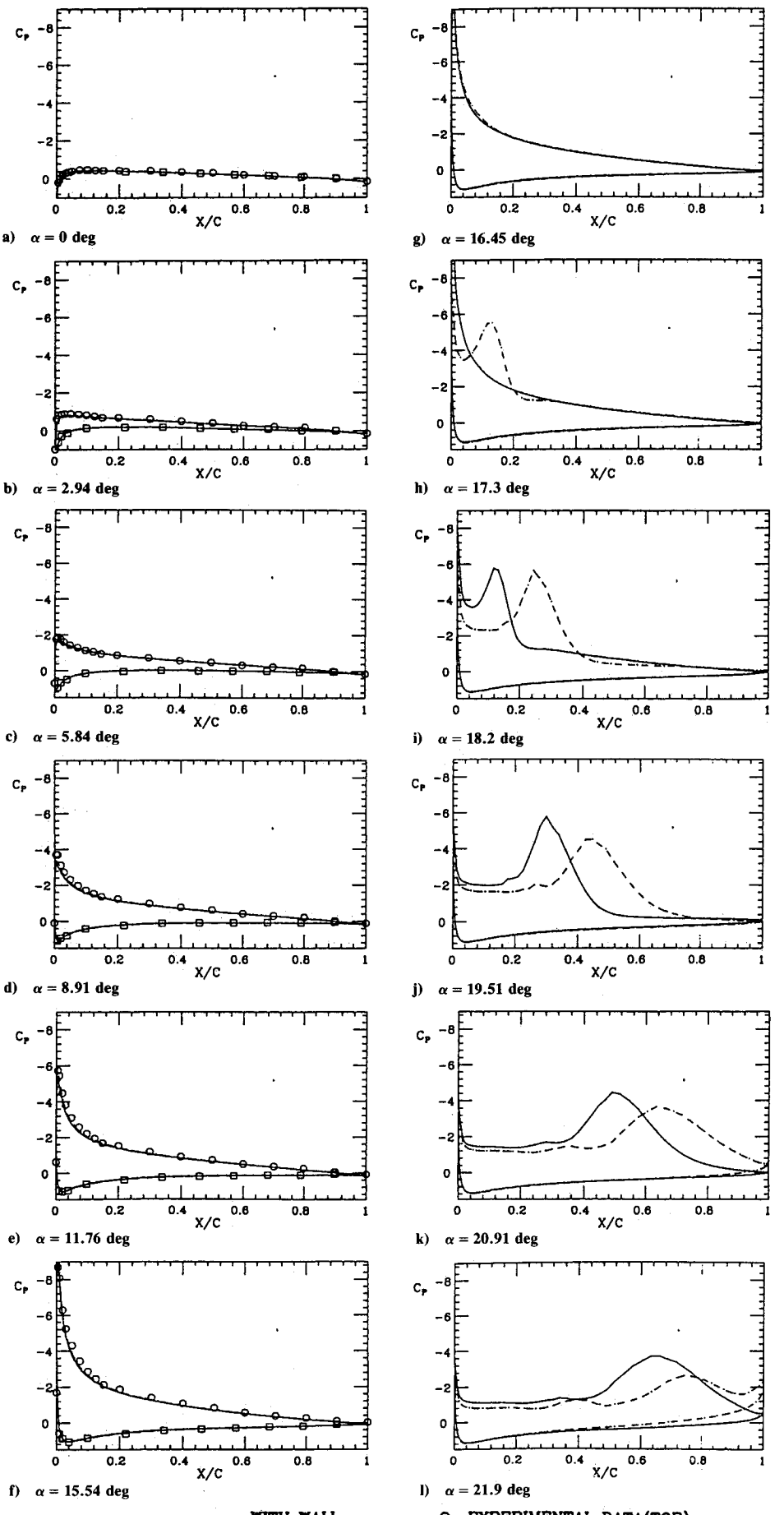

Fig. 5 Surface pressure coefficients distribution for dynamic stall at $M_\infty = 0.3$, $Re = 2.7 \times 10^6$, and $\kappa = 0.02546$.

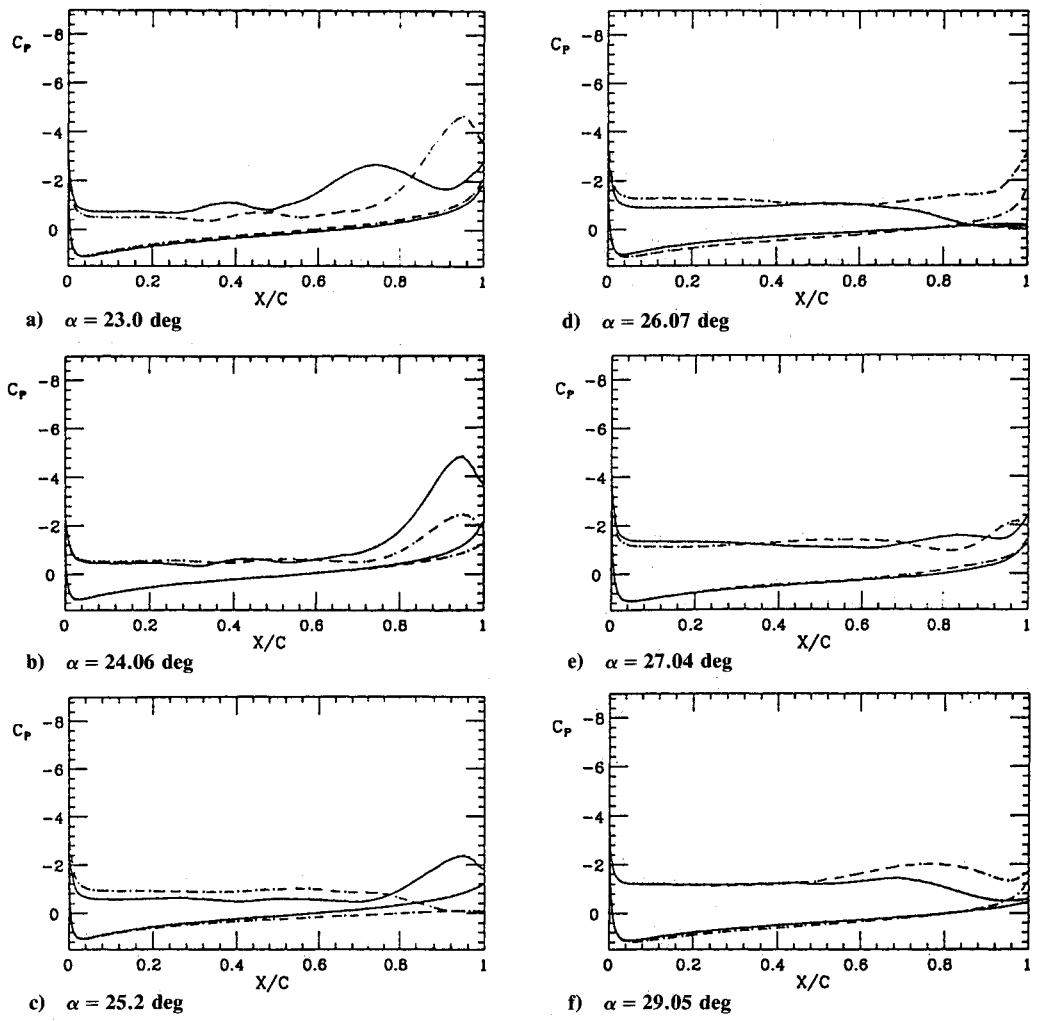

Fig. 6 Surface pressure coefficients distribution after dynamic stall at $M_\infty = 0.3$, $Re = 2.7 \times 10^6$, and $\kappa = 0.02546$.

Although identical solutions are obtained, the applications of the PSUG and DSUG approaches differ in the following aspects. The coding for the PSUG approach is less complex than for the DSUG approach. The stationary part of the unstructured grid for the PSUG approach does not require computation of new metrics at each step. The only extra work in addition to updating the inner grid is interpolation along the slip boundary. For the DSUG approach, the unstructured grid is computed each time as the angle of attack is updated requiring additional memory for the transient data and metrics. The number of steps required in subiterations (such that $\hat{Q}^l \rightarrow \hat{Q}^{n+1}$) for the DSUG approach is between 20–30% less than for the PSUG approach. However, the CPU time required for the DSUG approach for the whole pitch-up history is at least one third more than that for the PSUG approach. This can be attributed to the grid updating and metrics computation at each angle of attack for the DSUG approach.

Case 2: $M_\infty = 0.3$, $Re = 2.7 \times 10^6$, $\kappa = 0.01492$

For resolving the unsteady boundary layer, the C grid around the airfoil is refined to include 141×31 grid points. The unstructured grid contains 1190 cells and 733 nodes. The other structured grids are the same as the inviscid grids. The numerical computation is carried out up to $\alpha = 30$ deg, whereas experimental data are only available from $\alpha = 0$ to 15 deg.

Pressure coefficient distribution photographs are presented in Figs. 5a–5l. Excellent agreement with the experimental data can be seen for angle of attack up to 15.54 deg. This is true for approximations both with wall effect and without wall effect.

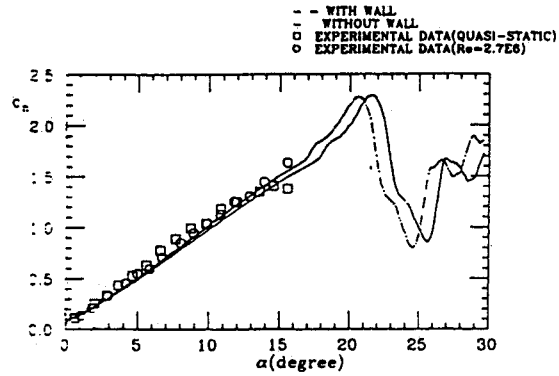

Fig. 7 Normal force coefficient hysteresis vs angle of attack for dynamic stall simulation at $M_\infty = 0.3$, $Re = 2.7 \times 10^6$, and $\kappa = 0.02546$.

As the angle of attack is increased to greater than 16.45 deg (Figs. 5f–5l), a significant difference is noticed between the leeward (upper surface) C_p of the with-wall and without-wall approximations. At $\alpha = 17.3$ deg (Fig. 5h), the leeward C_p of the with-wall approximation near the leading edge becomes more positive, and a local maximum (drop) and minimum (peak) are observed at $x/c = 0.04$ and 0.12, respectively. This suggests a leading-edge separation for the with-wall data. A similar curve is observed for the without-wall case in Fig. 5i. Moreover, the overall C_p distributions for the without-wall approximation evolve similarly to those of the with-wall ap-

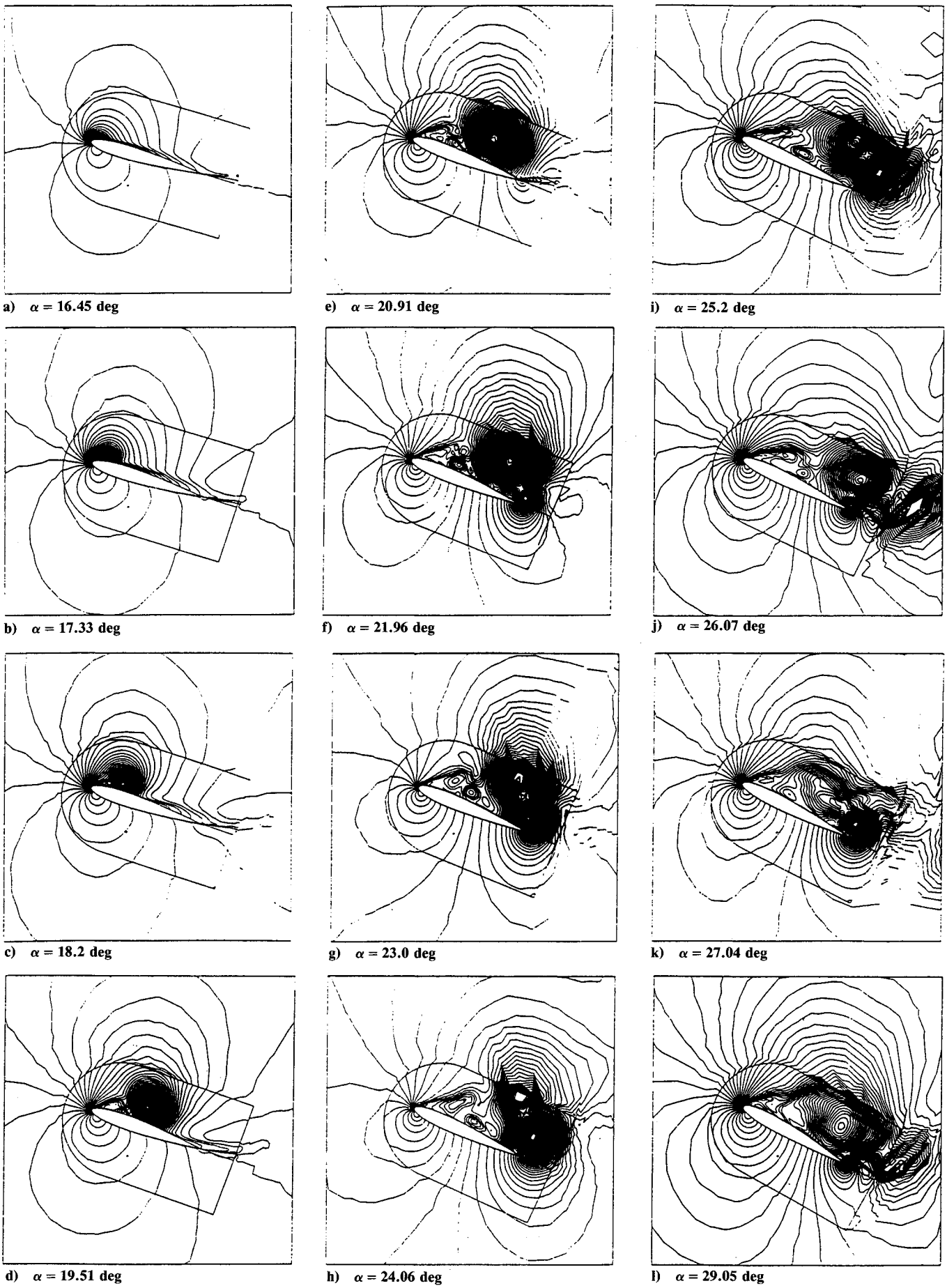

Fig. 8 Density contour of the dynamic stall at $M_\infty = 0.3$, $Re = 2.7 \times 10^6$, and $\kappa = 0.02546$.

proximation as the angle of attack increases (Figs. 5h–5l), except they are slightly delayed.

For both the with-wall and without-wall approximations, it is seen that the peak in leeward C_p (started in Fig. 5h or 5i) moves downstream as the angle of attack increases. It is also shown in Figs. 5h–5l that the peaks in leeward C_p distribution result in a larger overall difference in windward and leeward curves comparing to those of $\alpha = 16.45$ deg (Fig. 5g). This clearly indicates that there is an increase in lift (net area of C_p distribution) after the leading-edge separation. However, it is observed in Figs. 6a–6f that, as the peaks of the leeward C_p move close to the trailing edge, the net area becomes smaller. In particular, at $\alpha > 25.05$ deg, these peaks are hardly noticeable.

The phenomena observed in the C_p distribution plots are also demonstrated in Fig. 7, the history of the normal force coefficient. In this plot, both approximations (with wall and without wall) are plotted for angle of attack up to 30 deg. For the range $\alpha < 15$ deg, where experimental data are available, it can be seen that there is a good agreement between the measurements and the numerical data. In addition to predicting the linear relationship between C_n and α, the with-wall approximation is shown to be closer to the experimental data than the without-wall approximation. Most important, both of the numerical approximations show significant overshoots of the normal force coefficient (comparing to the quasistatic C_n maximum) at angle of attack after the leading-edge separation has occurred. This maximum C_n is 2.3, 64% greater than the quasistatic value. The angle at which the maximum C_n occurs is 21.5 deg (without wall), which is 6.5 deg higher than the α_{qs}. That is, the dynamic pitch-up allows a 6.5-deg margin after the quasistatic stall angle, and it yields an additional 64% normal force coefficient. It is also interesting to note that up to 5 deg after the dynamic stall both approximations (with and without wall) exhibit similar features except one lags the other by a maximum of 2 deg.

Figure 8 shows a sequence of plots of density contours for the with wall approximation ranging from $\alpha = 16.45$ to 29.05 deg. It can be seen that, after the leading-edge separation (Fig. 8b), a vortex develops at the leading edge (shown by concentric contour levels in Fig. 8c, $\alpha = 18.2$ deg). This vortex moves downstream and becomes bigger as the angle of attack increases (Figs. 8c–8f). It is also referred to as the leading-edge vortex in dynamic stall. As the leading-edge vortex reaches the vicinity of the trailing edge (Fig. 8g), it is seen to interact with a newly developed trailing-edge vortex. This phenomenon is first observed at $\alpha = 22$ deg, an angle of attack close to the dynamic stall. In Figs. 8h–8l, the trailing-edge vortex is seen to become bigger and the leading-edge vortex more diffused. Eventually, this vortex system moves downstream from the trailing edge (Fig. 8j). In Fig. 8k ($\alpha = 26.1$ deg), another vortex is developed at the trailing edge and the same process as was just described is seen to repeat (Fig. 8l). It should be mentioned that there are other small vortices observed in the sequence of plots. However, we only concentrate on the main features that govern the flow behavior.

As mentioned in the introduction, our numerical solutions will be used to predict the wall effect and compared to the PIDV flowfield measurements. In addition to the data shown here, other flow properties are readily extracted from these solutions. Ultimately, the numerical simulation and experimental measurements will complement each other in analyzing and understanding dynamic stall.

Conclusions

A hybrid grid Navier-Stokes approach is developed to study dynamic stall over an airfoil including wind-tunnel wall effect. Although it takes more CPU time in grid updating, the DSUG approach is more efficient than the PSUG approach in subiterations convergence. Good agreement is obtained between solutions and available experimental data. The unsteady vortical flow phenomena are captured, and they provide insight into the physics associated with dynamic stall.

Acknowledgment

This work is supported by the Supercomputer Computations Research Institute at the Florida State University, which is partially supported by the U.S. Department of Energy under Contract DE-FC05-85ER250000.

References

[1]Shih, C., Lourenco, L., and Krothapalli, A., "PIDV: An Integrated Tool for the Measurement of Unsteady Separated Flows," *ASME Symposium on Non-Steady Viscous Flows,* Toronto, June 1990.

[2]Landon, R. H., "NACA0012 Oscillatory and Transient Pitching," *Compendium of Unsteady Aerodynamic Measurements,* AGARD Rept. 702, Aug. 1982.

[3]McCroskey, W. J., McAlister, K. W., Carr, L. W., Pucci, S. L., Lambert, O., and Indergand, R. F., "Dynamic Stall on Advanced Airfoil Sections," *Journal of American Helicopter Society,* July 1981, Vol. 26, No. 3, pp. 40–50.

[4]Visbal, M. R., "Effect of Compressibility on Dynamic Stall of a Pitching Airfoil," AIAA Paper 88-0132, Jan. 1988.

[5]Carr, L. W., Chandrasekhara, M., Ahmed, S., and Brock, N., "A Study of Dynamic Stall Using Real Time Interferometry," AIAA Paper 91-0007, Jan. 1991.

[6]Lohner, R., "Adaptive Remeshing for Transient Problems," *Computer Methods in Applied Mechanics and Engineering,* Vol. 75, 1989, pp. 195–214.

[7]Thomas, J. L., Walters, R. W., Reu, T., Ghaffari, F., Weston, R. P., and Luckring, J. M., "A Patched-Grid Algorithm for Complex Configurations Directed Towards the F/A-18 Aircraft," AIAA Paper 89-0121, Jan. 1989.

[8]Meakin, R. L., and Suhs, N. E., "Unsteady Aerodynamic Simulation of Multiple Bodies in Relative Motion," AIAA Paper 89-1996, June 1989.

[9]Rai, M. M., "Unsteady Three-Dimensional Navier-Stokes Simulations of Turbine Rotor-Stator Interaction," AIAA Paper 87-2058, June 1987.

[10]Thomas, J. L., and Walters, R. W., "Upwind Relaxation Algorithms for the Navier Stokes Equations," AIAA Paper 85-1501, July 1985.

[11]Roe, P. L., "Characteristic Based Schemes for the Euler Equations," *Annual Review of Fluid Mechanics,* Vol. 18, 1986, pp. 337–365.

[12]Holst, T. L., Kaynak, U., Gundy, K. L., Thomas, S. D., Florest, J., and Chaderjian, N. M., "Transonic Wing Flows Using Euler/Navier-Stokes Zonal Approach," *Journal of Aircraft,* Vol. 24, No. 1, 1987, pp. 17–24.

[13]Baldwin, B. S., and Lomax, H., "Thin-Layer Approximation and Alegbraic Model for Separated Turbulent Flows," AIAA Paper 78-257, Jan. 1978.

[14]Anderson, W. K., Thomas, J. L., and Van Leer, B., "A Comparison of Finite Volume Flux Vector Splitting for the Euler Equations," AIAA Paper 85-0122, Jan. 1985.

[15]Reu, T., and Ying, S. X., "An Adaptive Multi-Coloring Scheme for Solving the Euler Equations on Unstructured Grids," *Proceedings of the Third International Conference on Numerical Grid Generation in CFD and Related Fields,* June 1991, pp. 391–402.

[16]Steger, J. L., and Sorenson, R. L., "Automatic Mesh-Point Clustering Near a Boundary in Grid Generation with Elliptic Partial Differential Equations," *Journal of Computational Physics,* Vol. 33, No. 3, 1979, pp. 405–410.

[17]Sloan, S. W., "A Fast Algorithm for Constructing Delaunay Triangulations in the Plane," *Adv. Eng. Software,* Vol. 9, No. 1, 1987, pp. 34–55.

[18]Mavriplis, D. J., "Adaptive Mesh Generation for Viscous Flow Using Delauney Triangulation," *Proceedings of the Numerical Grid Generation in CFD and Related Fields,* 1988, pp. 611–620.

[19]Batina, J. T., "Three-Dimensional Flux-Split Euler Schemes Involving Unstructured Dynamic Meshes," AIAA Paper 90-1649, June 1990.